AGU PUBLICATIONS

Water Resources Research

RESEARCH ARTICLE
10.1002/2015WR017664

Channel adjustments to a succession of water pulses in gravel bed rivers

Carles Ferrer-Boix[1] and Marwan A. Hassan[1]

[1]Department of Geography, University of British Columbia, Vancouver, British Columbia, Canada

Key Points:
- Experiments to a sequence of water pulses in poorly sorted sediment have been conducted
- Armor surface texture persists while bed structures partially vanish
- Bed load transport rates are related to the frequency of water pulses

Correspondence to:
C. Ferrer-Boix,
cfboix@geog.ubc.ca

Citation:
Ferrer-Boix, C., and M. A. Hassan (2015), Channel adjustments to a succession of water pulses in gravel bed rivers, *Water Resour. Res.*, *51*, 8773–8790, doi:10.1002/2015WR017664.

Received 5 JUN 2015
Accepted 15 OCT 2015
Accepted article online 21 OCT 2015
Published online 5 NOV 2015

Abstract Gravel bed rivers commonly exhibit a coarse surface armor resulting from a complex history of interactions between flow and sediment supply. The evolution of the surface texture under single storm events or under steady flow conditions has been studied by a number of researchers. However, the role of successive floods on the surface texture evolution is still poorly understood. An experimental campaign in an 18 m-long 1 m-wide flume has been designed to study these issues. Eight consecutive runs, each one consisting of a low-flow period of variable duration followed by a sudden flood (water pulse) lasting 1.5 h, have been conducted. The total duration of the experiment was 46 h. The initial bed surface was created during a 280 h-long experiment focused on the influence of episodic sediment supply on channel adjustments. Our experiments represent a realistic armored and structured beds found in mountain gravel bed rivers. The armor surface texture persists over the duration of the experiment. The experiment exhibits downstream fining of the bed-surface texture. It was found that sorting processes were affected by the duration of low-flow between flood pulses. Since bed load transport is influenced by sediment sorting, the evolution of bed load transport is impacted by the frequency of the water pulses: short interpulse durations reduce the time over which fine material (transported as bed load) can be winnowed. This, in turn, contributes to declining reduction of the bed load transport over time while the sediment storage increases.

1. Introduction

Channel morphology is influenced by the spatial distribution and the local organization of particles on river beds, which in turn result from interactions between the flow and the sediment supply (rate and texture). Nonlinear effects associated with sediment transport processes induce channel responses during flash flood events, which typically occur in mountain rivers and arid environments [e.g., *Pitlick*, 1994; *Alexandrov et al.*, 2007], that differ from those during tranquil, steady flow events [*Hassan et al.*, 2006]. Low sediment supply regimes in mountain streams [*Church and Hassan*, 2002] can be disturbed by large, episodic sediment injections when channels and hillslope are coupled. The frequency and amount of material entering the river can disturb sediment supply regimes, leading to diverse channel adjustments [*Madej*, 2001] that affect both the evolution of in-channel sediment storage and bed-surface texture [*Hassan et al.*, 2005, 2008; *Madej et al.*, 2009; *Pryor et al.*, 2011].

The bed texture of gravel bed rivers is usually characterized by the presence of a coarse armor. Of interest for sediment transport predictions and channel stability is to understand whether an armored surface vanishes or persists under flood conditions. Some field and experimental studies [*Dietrich et al.*, 1989; *Kuhnle*, 1989; *Lisle et al.*, 1993; *Ryan et al.*, 2005; *Vericat et al.*, 2006; *Wang and Liu*, 2009] suggest that surface armor is destroyed during floods. This results in a finer surface texture and a reduction of the armor ratio (the ratio between the median size of the surface and that of the subsurface) during floods. By contrast, some studies suggest that an armored bed surface persists during floods [*Andrews and Erman*, 1986; *Church and Hassan*, 2002; *Clayton and Pitlick*, 2008]. Numerical simulations [e.g., *Wilcock and DeTemple*, 2005; *Parker et al.*, 2008] have shown that an armored surface persists even during flood events. The persistence or breakup of surface armor during flood conditions has been explained within a unifying framework of the occurrence of mobile armor [*Parker et al.*, 1982; *Parker and Klingeman*, 1982], a coarse surface texture resulting from the overrepresentation of coarse and inherently less mobile particles on the surface so that equal mobility is achieved. This mobile texture gradually shifts toward the coarsest possible texture (static armor) or toward unarmored bed as flow strength (characterized by the boundary shear stress) respectively decreases or increases [*Parker*, 2008].

Although flow hydrographs likely impact sediment transport, and bed surface adjustments, their effects on river adjustments have been analyzed by only a few studies. Much of the work has been conducted on studying the hysteretic effects of bed load transport rates and textures during hydrograhs [e.g., *Lee et al*., 2004; *Hassan et al*., 2006; *Humphries et al*., 2012; *Mao*, 2012; *Guney et al*., 2013; *Martin and Jerolmack*, 2013; *Waters and Curran*, 2015]. Of interest for this research are (i) the interactions between the bed surface composition and the bed load transport (rate and texture) and (ii) the influence of antecedent conditions of the bed surface on sediment transport (rate and grain-size distribution) and channel adjustments during unsteady flows.

Hassan et al. [2006] observed bed load coarsening followed by a gradual fining of the bed load texture during the rising and falling limb of a hydrograph, respectively. These changes in the bed load composition were accompanied by surface texture adjustments which, in turn, were found to depend on the shape and the duration of the rising limb of the hydrographs [*Hassan et al*., 2006]. Particle rearrangement and bed surface restructuring during the falling limb of hydrographs produced an increase of the reference shear stress and a consequent reduction of the sediment transport rates [*Mao*, 2012]. *Waters and Curran* [2015] reported sheltering effects produced by gravel on sand grains which in turn reduced entrainment rates contributing to stabilize the bed.

The influence of the antecedent bed-surface texture on sediment transport rates in unsteady flow events has been studied by a number of researchers. *Guney et al*. [2013] found that the higher the degree of coarsening of the surface prior to a hydrograph, the lower the sediment yield during the unsteady flow stage. *Reid et al*. [1985] reported that long time periods of low flow between floods enhanced particle interlocking and infiltration of fine material below the surface, increasing the strength of the bed framework and ultimately leading to a reduction of sediment transport rates. Long durations of antecedent low flow contributed to consolidate and stabilize the bed, which in turn prevented particle entrainment [*Waters and Curran*, 2015] by allowing more time for particles to be rearranged locally into a more stable configuration [*Haynes and Pender*, 2007]. Further, *Waters and Curran* [2015] suggested that the lack of a clear trend in the hysteretic relations between the flow and the sediment transport (clockwise or counterclockwise) might be partly due to the antecedent conditions of the bed surface. Particle reorientation [*Ockelford and Haynes*, 2013], clustering [*Reid et al*., 1985], imbrication and packing of surface grains [e.g., *Reid et al*., 1985; *Haynes and Pender*, 2007; *Ockelford and Haynes*, 2013], and bed structuring [*Church et al*., 1998; *Hassan and Church*, 2000; *Oldmeadow and Church*, 2006] also contribute to increasing bed stability.

Except the field study carried out by *Reid et al*. [1985], most of the contributions have focused on different aspects of the fundamental response of gravel bed rivers to single hydrographs. Therefore, channel adjustments to a sequence of floods affects still remain an open question.

An experimental campaign aimed to study channel adjustments under different episodic sediment supply regimes was conducted at Department of Geography at the University of British Columbia [*von Flotow*, 2013; *Elgueta*, 2014]. The complex history of sediment supply during this experiment resulted in a channel with a structured and armored bed surface and a significant amount of sediment storage, primarily as a wedge of sediment near the inlet and as bars farther downstream. These conditions resemble those found in mountain streams [e.g., *Reid et al*., 1985; *Church et al*., 1998; *Hassan and Church*, 2000; *Oldmeadow and Church*, 2006]. Thus, this configuration offers an opportunity to study how an armored, structured bed surface, typical of upland gravel bed rivers, responds to a series of successive floods (water pulses). An experimental campaign was designed with the objective of determining the influence of flood magnitude and frequency on mobilizing (i) sediment accumulated in the channel and (ii) the coarse particles on the bed surface. These experiments consist of a succession of runs, each one consisting of a low-flow period followed by a sudden increase in the water discharge (pulse). The manuscript is structured as follows. First, we describe the experimental campaign (summarizing also the conditions of the previous runs that were used as initial condition for our experiment). Second, we describe the most important results of the experiments, focusing on the response of the surface texture, bed load transport (rate and texture), and the bed profile to a succession of water pulses. Finally, a discussion follows on the processes associated with the surface texture evolution.

2. Experimental Arrangements

Flume experiments were carried out in the Department of Geography at the University of British Columbia. Experiments were conducted in an 18 m-long, 1 m-wide and 1 m-deep tilting flume.

Table 1. Sediment Supply Conditions and Feed Rates of the Previous Experiment

Run	1	2	3	4	5	6	7
Feed	No feed	Constant	1 pulse	4 pulses	2 pulses	Constant	No feed
$q_{b,f}$ (g/m/s)	0	2.1	83	83	83	2.1	0

2.1. Initial Conditions: Surface Texture and Sediment Supply

We conducted our experiment as part of a major project examining the impact of episodic sediment supply on bed evolution and channel adjustment. A brief description of these experiments is given below. More details can be found in *von Flotow* [2013] and *Elgueta* [2014]. Seven consecutive runs, each lasting 40 h, were conducted under constant flow (65 L/s) but varying sediment supply rates for a total duration of 280 h (Table 1 and Figure 1). The feed texture (Figure 2) was identical to that of the original mixture with a bed slope of 0.0218 m/m. After 280 h, the bed surface was well armored with a mean particle size of 17 mm, an armor ratio based on the ratio between the geometric mean grain size of the surface $D_{g,s}$ and that of the subsurface $D_{g,bulk}$ of 2.7 (Figure 2) and well developed pebble clusters and surface structures [*von Flotow*, 2013]. This final bed surface constituted the initial configuration for our experiments (Figure 2). Over the course of the experiment, a net accumulation of 494 kg of sediment was stored in the channel, part of it in a wedge of sediment near the feed zone (between x = 11.5 m and x = 12.5 m in Figure 2) and the rest in downstream bars [*Elgueta*, 2014]. Figure 1b shows the mean longitudinal profiles obtained after 40 and 280 h. The bed slope of this latter profile was $S_0 = 0.022$ m/m. The average thickness of sediment along the flume was 10 cm. This experiment, hereafter referred to as "previous experiment," provided the initial surface and longitudinal profile for the experiments presented herein.

2.2. Water Pulses Experiment

The flume slope was set constant at 0.022 m/m for all runs. Due to laboratory constraints, the working length of the flume was set to 13 m. A poorly sorted sediment with a density of 2650 kg/m^3, identical to the sediment mixture texture, was used as feed material (Figure 2). Sediment was introduced by hand into the flume 13 m upstream of the channel outlet at a constant sediment rate of 2.1 g/m/s.

The material that composed the bed extended approximately 0.5 m upstream of the feeding station. Upstream of this point, the bed was covered with fixed particles having the same texture as the rest of the bed. In each run, water discharge consisted of a constant low-flow period of variable duration (Δt_{LF}), followed by a constant high-flow period that lasted 1.5 h (Figure 3). Low-flow and high-flow (pulse) discharges were 65 and 91 L/s, respectively (Table 2). Eight consecutive runs were conducted; the surface texture and the bed configuration at the end of each run constituted the initial conditions for the subsequent run. The low-flow period Δt_{LF} ranged from 10 h (runs 1 and 2) to 1 h (runs 5–8). The total duration of all runs was 46 h (Figure 3 and Table 2). Table 2 summarizes the most important variables for each run, distinguishing between low flow and pulses.

The geometric mean diameter and the geometric standard deviation of the mixture were $D_g = 5.65$ mm and $\sigma_g = 3.05$, respectively (Figure 2). Grain size ranged from 0.5 to 64 mm, with a sand content of about

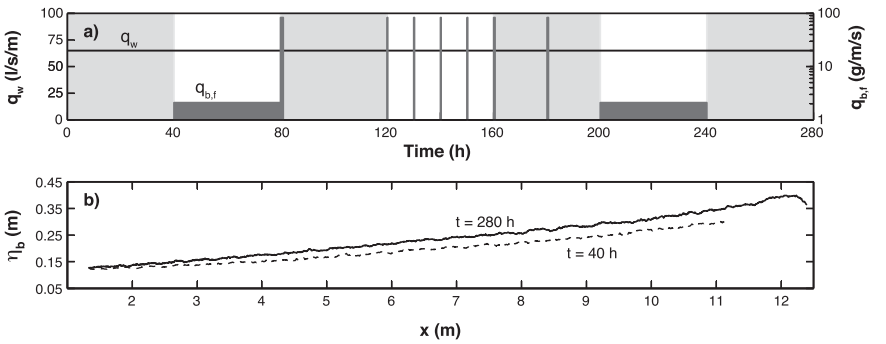

Figure 1. (a) Water discharge and sediment supply regime throughout the previous experiment. (b) Mean longitudinal profiles at t = 40 h and t = 280 h. Flow is from right to left. q_w: water discharge per unit width; $q_{b,f}$: feed rate per unit width; and η_b: mean bed elevation.

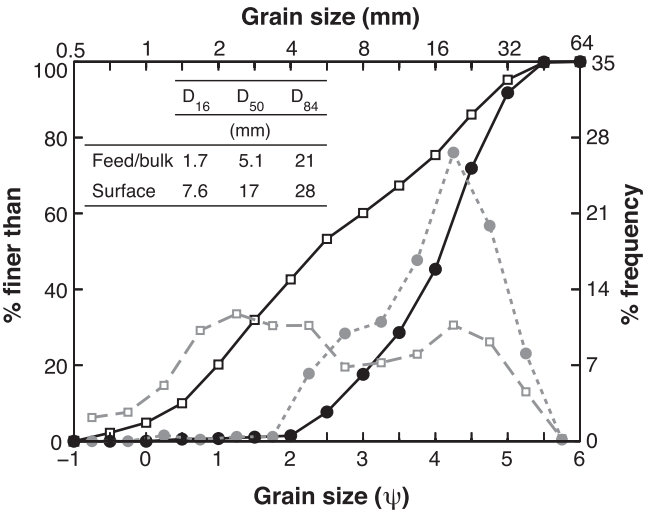

Figure 2. Textures of the bulk/feed (open squares) and the initial bed surface (filled circles) used in these experiments. Percent finer curves (black lines, left vertical axis) and percentages of the surface frequencies (grey lines, right axis) are presented.

20% (Figure 2). Each grain size was painted in a different color at $1/2-\psi$ intervals ($\psi=\ln(D)/\ln 2$, i.e., $\psi=-\phi$, being ϕ the sedimentological grain scale).

The width and slope of the flume and the feed/bulk texture used represent a generic 1 : 3 model (Froude similarity) of a riffle-pool sequence in East Creek, British Columbia [*von Flotow*, 2013; *Elgueta*, 2014]. Water discharges at low-flow and during high-flow pulses were equivalent to the bankfull discharge and a discharge 40% higher than bank full in East Creek, respectively. Therefore, "low flow" and "high flow" are just notation and are used hereafter in the paper to denote the lowest and the highest of the two flow rates considered. The temporal sequence of high-flow pulses was chosen to study the influence of the duration of low flows on channel adjustments and it does not reflect specific hydrological records at East Creek. Therefore, although the experiment is based on physical characteristics of East Creek, it represents a general configuration of a typical mountain gravel bed river subjected to a series of successive floods.

Before starting each run, the flume was slowly saturated with flow well below that needed to initiate motion. Water discharge was then gradually increased to the desired value. Once the desired value was achieved, sediment was fed into the channel.

The bed and water surface profiles were periodically measured during the runs with vertical rulers attached to the glass of the flume at about 0.5 m intervals between x = 1 m to x = 13 m, being the flume outlet at x = 0 m (Figure 3). No water depth constraint was imposed at the downstream end of the flume.

Mean shear stresses acting on the bed surface were obtained by means of the depth slope product. Mean water surface slopes and the hydraulic radius between longitudinal coordinates x= 5 m and x = 11 m were used. Sidewall effects were removed using the procedure proposed by *Vanoni* [1975].

A sediment trap was placed at the downstream end of the flume; it was equipped with a load cell so that the cumulative mass of sediment leaving the flume was registered continuously at 0.1 s intervals. Bed load transport rate was calculated using finite differences by filtering the cumulative mass at 120 s intervals. Spurious negative values of computed transport were discarded. Relative errors between the filtered results and the raw mass measurements for the entire experiment range between 3.6% and 3.7% (i.e., 4% for

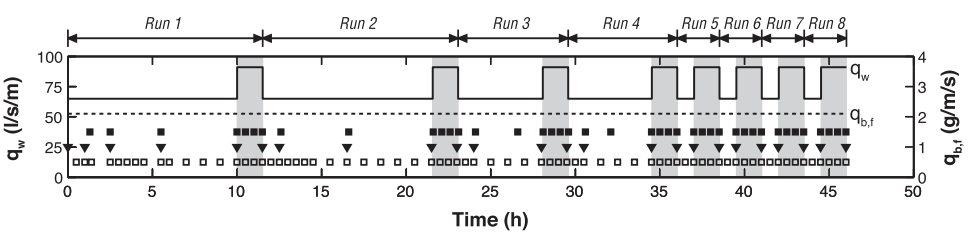

Figure 3. Temporal distribution of (i) the water discharge during the complete series of consecutive runs (continuous line, left vertical axis) and (ii) sediment feed rate (dashed horizontal line, right axis). Vertical grey patches depict the water pulses of 1.5 h (the same patches are used in subsequent figures to identify water pulses). Markers illustrate the time at which different measurements were done: (i) open squares, bed and water surface elevation profiles, (ii) black-filled squares, bed load from the sediment trap, and (iii) black-filled triangles, bed scans and bed-surface texture.

Table 2. Summary of the Most Important Experimental Variables for Each Run (Distinguishing Between Low-Flow and High-Flow Periods)[a]

Run	q_w (m^2/s)	Δt (h)	S_0 (m/m)	H (m)	τ_b (Pa)	$D_{g,s}$ (mm)	q_b (g/m/s)	$D_{g,b}$ (mm)
1	0.065	10	0.0240	0.071	15.8	15.1	0.26	5.8
	0.091	1.5	0.0219	0.093	19.6	14.7	6.79	5.3
2	0.065	10	0.0224	0.080	14.0	14.9	0.71	4.3
	0.091	1.5	0.0217	0.096	16.8	15.5	5.71	4.7
3	0.065	5	0.0222	0.079	13.0	15.2	0.60	3.5
	0.091	1.5	0.0217	0.090	15.3	15.7	4.15	5.0
4	0.065	5	0.0219	0.079	13.2	14.9	0.50	3.4
	0.091	1.5	0.0215	0.089	15.7	15.6	2.73	5.1
5	0.065	1	0.0217	0.075	11.8	15.7	0.89	3.1
	0.091	1.5	0.0216	0.092	15.6	15.9	3.66	5.1
6	0.065	1	0.0217	0.076	12.6	15.9	1.09	4.6
	0.091	1.5	0.0216	0.091	15.9	15.6	1.34	4.5
7	0.065	1	0.0218	0.078	12.8	15.6	0.64	4.2
	0.091	1.5	0.0216	0.094	15.6	16.6	1.51	5.0
8	0.065	1	0.0217	0.081	13.4	15.8	0.80	4.7
	0.091	1.5	0.0214	0.090	15.1	16.0	1.23	4.9

[a] q_w: water discharge per unit width; Δt: duration of each run; S_0: mean bed slope; H: mean water depth; τ_b: mean boundary shear stress action on the bed surface; $D_{g,s}$: mean geometric mean size of the bed surface; q_b: mean sediment transport rate at the outlet; $D_{g,b}$: mean geometric mean size of the bed load transport; feed rate per unit width $q_{b,f}$ was kept constant throughout the experiment to 2.1 g/m/s.

practical purposes) for time windows varying from 1 to 300 s, suggesting that potential errors introduced by data filtering were minor. The maximum relative differences in mass between filtered results and raw measurements were registered during the first 10 h at low flow when the cumulative mass of sediment was $<$6 kg (the maximum mass deviation for the whole experiment ranges between 4.3 and 4.7 kg, obtained at $t \approx 45$ h when the total cumulative mass of sediment was around 198 kg). Periodically, the water pump was turned off, the sediment feed was interrupted, the flume was drained, and the sediment trap was emptied and replaced to obtain the grain-size distribution of the collected bed load. Thus, the texture of the material trapped at a given time is a lumped representation of the bed load transport rate of the period of time during which the trap was filled.

To determine the particle size distribution of the bed surface along the working length of the flume, a photographic method was used at various time intervals (Figure 3). A camera was mounted on top of the flume and 15 images (0.7 m apart) of the bed were taken. Each surface image covered approximately 1 m of the bed, with an overlap around 0.2 m on adjacent photographs. Each image was sampled by using an adaptation of the Wolman method based on color coded sediment at 1/2 ψ intervals [*Zimmermann et al.*, 2010]. One hundred four particles per image were sampled, providing a noninvasive characterization of the bed texture along the entire flume. Due to the shadows cast by large clasts, particles $\leq$2 mm were excluded; these particles represented, on average, 8% of each image. Bed surface elevation was also obtained by means of laser scans at a resolution of 2 $\times$ 2 mm [*Zimmermann et al.*, 2010]. Therefore, a digital elevation model (DEM) of the bed was obtained at each measuring time. As detailed below, DEMs were used to determine the longitudinal profile of the flume. A 5 cm-wide buffer was set on each side of the flume to avoid measurement errors near the walls. Mean bed elevations were obtained after averaging the two-dimensional scan in the transverse direction. Detrended bed surfaces have been obtained from bed scans. The bed surface of the channel, which had a three-dimensional structure, i.e., it presented zones of upward or downward bed elevation along the longitudinal and/or transverse directions, was divided into 1 m-long and 0.3 m-wide regions. Mean local bed slopes in the Cartesian directions were obtained for each region. Therefore, a mean bed surface was obtained for each region. Detrended bed surface of the channel was then obtained after subtracting the mean bed surfaces from the original bed scans. Mean detrended longitudinal profiles were computed after averaging detrended surfaces in the transverse direction.

3. Results

The evolution of the surface grain-size distribution throughout the experiment is presented first, followed by bed load transport rates and compositions, and finally the evolution of the bed profile and the development of bed forms.

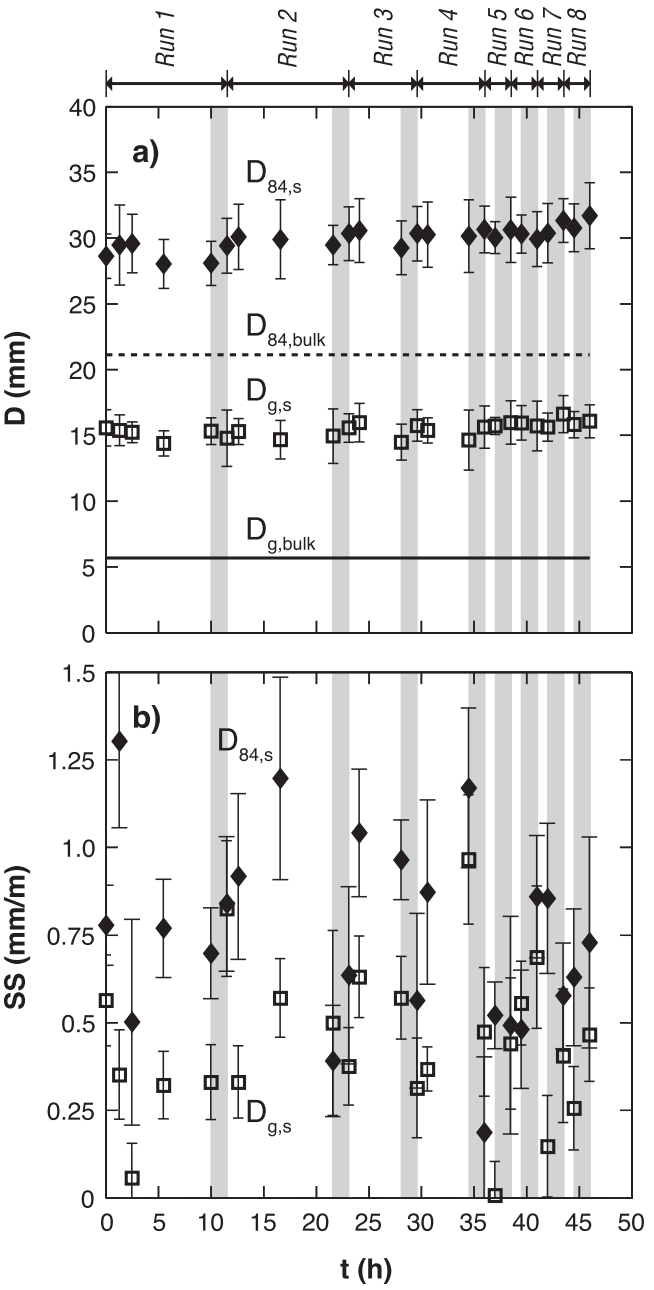

Figure 4. (a) Temporal evolution of the mean geometric grain size and the 84 percentile of the bed surface, $D_{g,s}$ and the $D_{84,s}$, respectively. Vertical bars span $\pm\sigma$ around the mean value of D. Horizontal continuous and dashed lines depict the values of the D_g and the D_{84} of the bulk material. (b) Temporal evolution of the dimensionless sorting slope SS associated with $D_{g,s}$. Vertical lines indicate the mean absolute errors of between the grain size obtained with the interpolated sorting slopes and the grain sizes along the flume averaged by the working length. In both parts: geometric mean grain size (open squares) and 84 percentile (black diamonds).

3.1. Surface Texture: Armor Ratios and Longitudinal Sorting

Due to the previous experiment [*von Flotow*, 2013; *Elgueta*, 2014], the bed surface was significantly coarser than the bulk material, with an armor ratio of 2.7 (at t = 0 h, Figure 2). During the first run, we observed slight changes in the bed-surface texture (Figure 4a). After the first water pulse, the surface texture fined slightly: $D_{g,s}$ decreased about 4% decrease (Figure 4a). Overall however, the bed surface coarsened slightly after each water pulse, especially for runs 2–4 (Δt_{LF} = 10–5 h) (Figure 4a); armor ratios of the geometric mean size were 4%, 9%, and 7% coarser than the texture at low flow for each run. Except for run 7, in which 6% coarsening in the geometric mean size was recorded, much less coarsening is noticed for the last four runs (Δt_{LF} = 1 h). For example, only 1% fining was observed in run 6 and less than 2% coarsening for runs 5 and 8.

Longitudinal sorting was evaluated using the mean slope, hereafter denoted as sorting slope, SS of the geometric mean size $D_{g,s}$ and the D_{84} along the study reach (Figure 4b), which were obtained by linear regression. SS therefore represents the longitudinal variation of a grain size is along the flume. SS > 0 indicates downstream fining (grain size coarsens in the upstream direction); conversely, SS < 0 represents downstream coarsening of the bed-surface texture. Finally, SS = 0 denotes a bed surface whose grain size does not change longitudinally. Analogous interpolation schemes were used to analyze the sediment sorting in channels [*Seal et al.*, 1997] and dunes and Gilbert-type deltas [*Kleinhans*, 2005; *Ferrer-Boix et al.*, 2014]. Downstream fining (positive SS) was observed throughout the runs (Figure 4b). In general (21 out of 24 measurements), sorting slopes associated with variations in $D_{84,s}$ were greater than those associated with the variations of $D_{g,s}$. The averaged SS associated with $D_{g,s}$ during the first low-flow period was 0.3 mm/m. This implies that the mean difference in $D_{g,s}$ between the uppermost and the lowermost sections of the study reach represented 10% of the averaged $D_{g,s}$ within the reach (Figure 4a). The first pulse increased the sorting slope (greater downstream fining) of $D_{g,s}$ so that the difference between the upstream and downstream surface samples with respect to the mean $D_{g,s}$ of the reach was 30%. High flows of runs 2–4 (Δt_{LF} = 10–5 h) decreased sorting slopes associated with $D_{g,s}$: the mean

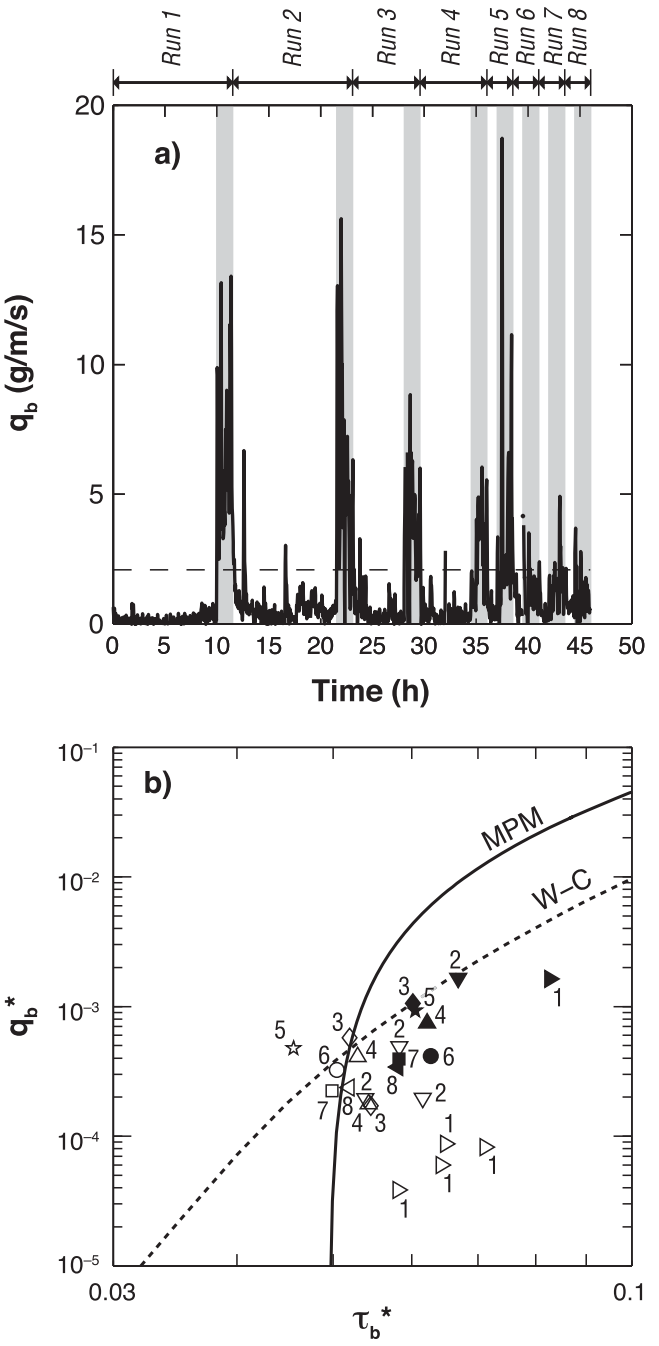

Figure 5. (a) Bed load transport rate per unit width of channel throughout the experiment. The dashed horizontal line represents the sediment feed rate. (b) Time-averaged dimensionless sediment transport rate q_b^* as a function of the Shields number τ_b^* associated with the mean geometric grain size of the bed surface. The black curve labelled MPM in Figure 5b illustrates the sediment transport capacity according to Meyer-Peter and Müller as corrected by *Wong and Parker* [2006]. Open and filled markers refer to low-flow periods and water pulses, respectively. Adjunct numbers in Figure 5b denote the measurements of each run.

sorting slopes for these three runs at low flow and during pulses were 0.6 and 0.4 mm/m, respectively. An opposite trend was observed for the last four pulses ($\Delta t_{LF} = 1$ h), when SS indicates fining of the surface material in the downstream direction: mean SS at low flow and during pulses for these latter four runs was 0.2 and 0.5 mm/m, respectively.

3.2. Sediment Transport: Rates and Textures

Higher sediment transport rates were observed during high-flow pulses than during low-flow periods (Figure 5a). However, averaged bed load rates during pulses declined in time (from 6.74 g/m/s for the first pulse to 1.22 g/m/s for the last, Table 2). This gradual declining trend was not followed during run 5, in which a high pulse in the bed load transport, likely due to a passage of a bed form or alternate bar, was noticed. During the final three pulses, time-averaged bed load transport per run was approximately constant (mean value of 1.34 g/m/s). The sediment transport rate during the first 10 h at low flow remained well below the feed rate (Figure 5a and Table 2). A nearly threefold increase in the averaged sediment transport rate was observed at low flow in run 2 compared to run 1 (Figure 5a and Table 2). A gradual decline in the bed load transport was evident during the run 2 low-flow period. Some variations were observed in the averaged sediment transport rate among runs 2–8 under low-flow conditions: rates ranged from 0.50 to 1.09 g/m/s with a weighted average of 0.67 g/m/s (Table 2). The standard deviation of the mean sediment transport rate of each low-flow period was 0.2 g/m/s, being the coefficient of variation (COV), defined as the ratio between the arithmetic mean over the standard deviation, 0.27.

The dimensionless sediment transport rate associated with the geometric mean size of the bed load ($D_{g,b}$) size is given by

$$q_b^* = \frac{\bar{q}_b}{\sqrt{RgD_{g,b}}D_{g,b}} \quad (1)$$

where $\bar{q}_b$ is the averaged volumetric sediment transport rate per unit width during the time that the sediment trap filled and the grain-size distribution of the bed load obtained (Figure 3), R is the submerged specific gravity, and g is the gravitational acceleration. The dimensionless sediment shear stress (τ_b^*) associated with the geometric mean size of the bed $D_{g,s}$. τ_b^* is defined as

$$\tau_b^* = \frac{\tau_b}{\rho RgD_{g,s}} \quad (2)$$

where ρ is the water density. Higher values of the dimensionless shear stress τ_b^* were observed at pulses compared to those obtained at low flow (Figure 5b). The transport capacity formulae of Meyer-Peter and Müller (MPM), corrected by *Wong and Parker* [2006] and that by *Wilcock and Crowe* [2003] (W-C) are plotted for comparison—in this latter case, the texture of the initial surface texture has been used. The highest dimensionless shear stress ($\tau_b^* = 0.083$) was associated with the end of the first pulse. Lower shear stresses were associated with the rest of the pulses (other black markers in Figure 5b), with no significant changes over time (τ_b^* ranges from 0.057 to 0.066 during runs 2–8). The same range of shear stresses were recorded at low flow during run 1, when dimensionless sediment transport rates were more than 1 order of magnitude lower than those registered during pulses on runs 2–8 (Figure 5b). Shear stresses during low-flow periods for runs 2–8 were lower than those for run 1. Except for the first low-flow period, in which Meyer-Peter and Müller sediment transport capacity significantly overpredicts the measured bed load transport rates (by 2 or even 3 orders of magnitude), the rest of the measurements at low flow can be considered acceptable (contained in a range smaller than 1 order of magnitude). Less accurate predictions of the bed load transport are obtained at pulses.

Bed load textures, expressed as the 16th and 84th percentiles and $D_{g,b}$ of the bed load, during the first 5 h of run 1 were highly variable (Figure 6). The $D_{g,b}$ at the end of the first low-flow period was slightly coarser than that of the feed. However, the coarsest fraction of the distribution (characterized by the $D_{84,b}$) was finer than the feed.

If $D_{g,b}$ is taken as a proxy for the bed load texture, temporal analysis of the bed load texture during low-flow periods shows a gradual fining of the average bed load texture during each run: average $D_{g,b}/D_{g,f}$ equaled 0.90, 0.76, and 0.62 for runs 1, 2, and 3, respectively. $D_{g,b}/D_{g,f}$ remained fairly constant, oscillating around 0.62 during run 4 until run 5 when a slight decline to a value of 0.55 was noticed. Bed load texture at t = 39.5 (run 6) coarsened sharply ($D_{g,b}/D_{g,f} = 0.82$) and remained approximately constant for runs 7 and 8. $D_{16,b}$ and $D_{84,b}$ mimic the $D_{g,b}$ trend. These low-flow results imply that the coarsest sediment supplied was stored within the channel and did not leave the flume (Figure 6).

Bed load texture during high-flow pulses was coarser than that at low flow. However, these differences were only statistically significant for runs 4 and 5 (Kolmogorov-Smirnov goodness-of-fit tests between lumped low-flow and high-flow pulse textures are different at a significance level of 0.05). Bed load texture remained finer than the feeding material during high-flow pulses, hence coarse fractions of sediment still accumulated in the flume even at high flow. Bed load at the first pulse exhibited the coarsest recorded texture ($D_{g,b}/D_{g,f} = 0.95$). However, bed load texture remained approximately constant at a lower value for the rest of the pulses (its average ratio $D_{g,b}/D_{g,f} = 0.86$, standard deviation 0.034). Except for the first pulse, for which no significant differences in the bed load texture were observed (Figure 6a), bed load texture varied during pulses. Grain-size distributions of bed load transport progressively fined throughout water pulses. Bed load textures obtained 0.5 h after beginning of each pulse, i.e., the first of the textures sampled during pulses (Figure 6), were between 8% and 30% coarser than samples obtained at the end of a pulse (if $D_{g,b}$ is used to evaluate the degree of coarsening). Kolmogorov-Smirnov goodness-of-fit tests show however, that differences are not statistically significant for any of the pulses at a significance level of 0.05.

Fractional transport rates [*Wilcock and McArdell*, 1993] as applied by *Hassan et al.* [2006] and *Ferrer-Boix and Hassan* [2014] p_{bi}/f_i, i.e., the ratio between the bed load (p_{bi}) and the surface (f_i) frequencies, for runs 1 and 8 were obtained. Because grain sizes finer than 2 mm could not be identified from image analysis they have been discarded. Thus, p_{bi} and f_i have been renormalized considering only those fractions coarser than 2 mm. No significant differences in fractional transport throughout the experiment were noticed (Figure 7).

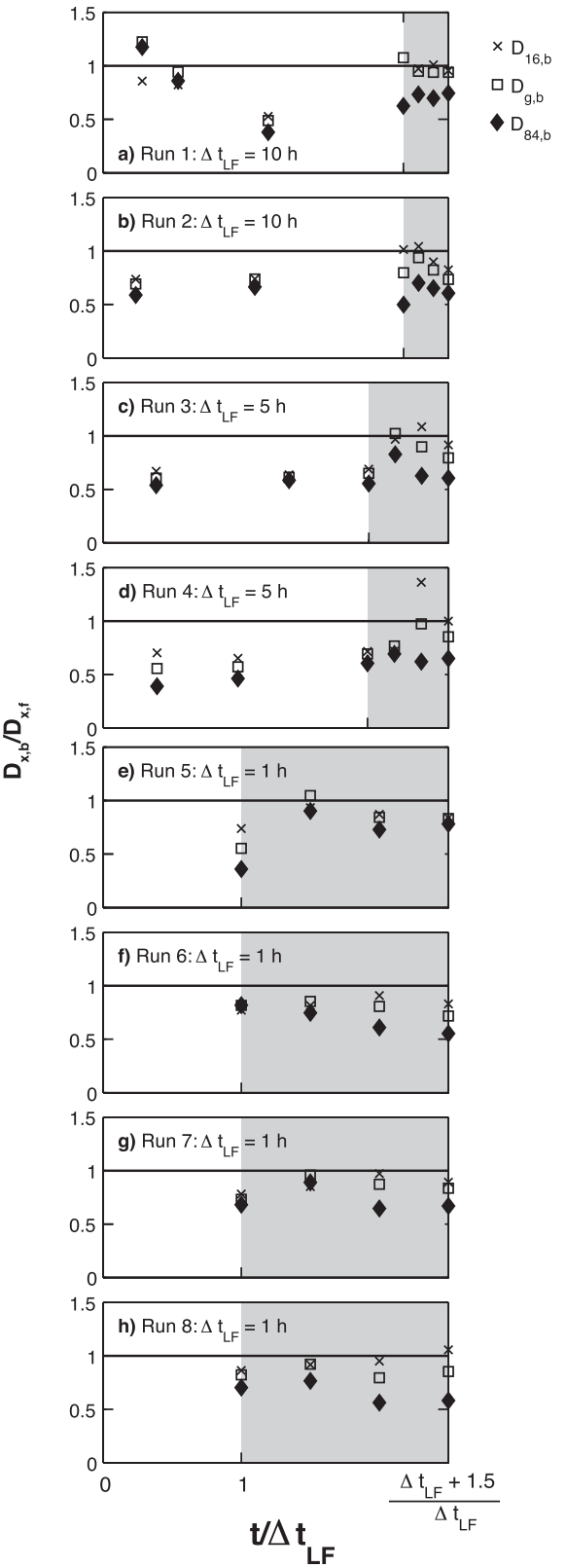

Figure 6. Ratio of the $D_{16,b}$ (crosses), $D_{g,b}$ (squares), and $D_{84,b}$ (black diamonds) of the bed load relative to those grain sizes $D_{x,f}$ of the feed. Black horizontal line indicates $D_{x,b} = D_{x,f}$. Relative time (abscissa axis) with respect to the starting time of the respective low-flow periods has been made dimensionless by dividing it by the duration of the low-flow period. Times and durations of the water pulses are depicted with grey patches. Note that the width of the water pulses varies among (a–h) according to the ratio between the duration of the water pulses (fixed and equal to 1.5 h) and the variable duration at low flow for the same run.

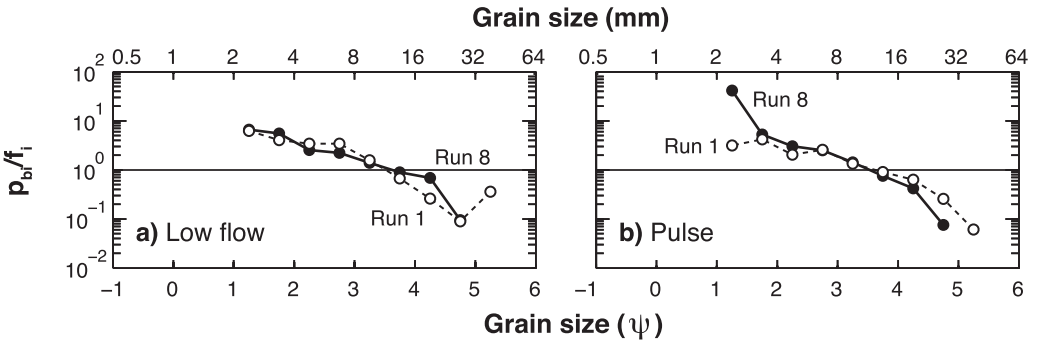

Figure 7. Fractional transport rates p_{bi}/f_i for runs 1 (open circles) and 8 (black circles) at the end of the respective (a) low-flow periods and (b) pulses. Dashed horizontal line in each part highlight full mobility ($p_{bi}/f_i = 1$).

3.3. Bed Profile and Bed Forms

Minor bed elevation changes ($\Delta\eta_b$) were observed in the mean bed profile of the flume along the channel (Figure 8a). The bed at low flow in run 1 alternated between periods of aggradation and degradation. However, cycles of bed aggradation and degradation observed during recurrent low-flow and high-flow pulses (Figure 8a) gradually waned with time (Figure 8b). Bed elevation changed little throughout the entire 10 h period: the net change in bed elevation was −0.27 mm. It was during the first pulse when the most important changes in the bed elevation occurred: 6.6 mm of degradation on average, which represented 40% of

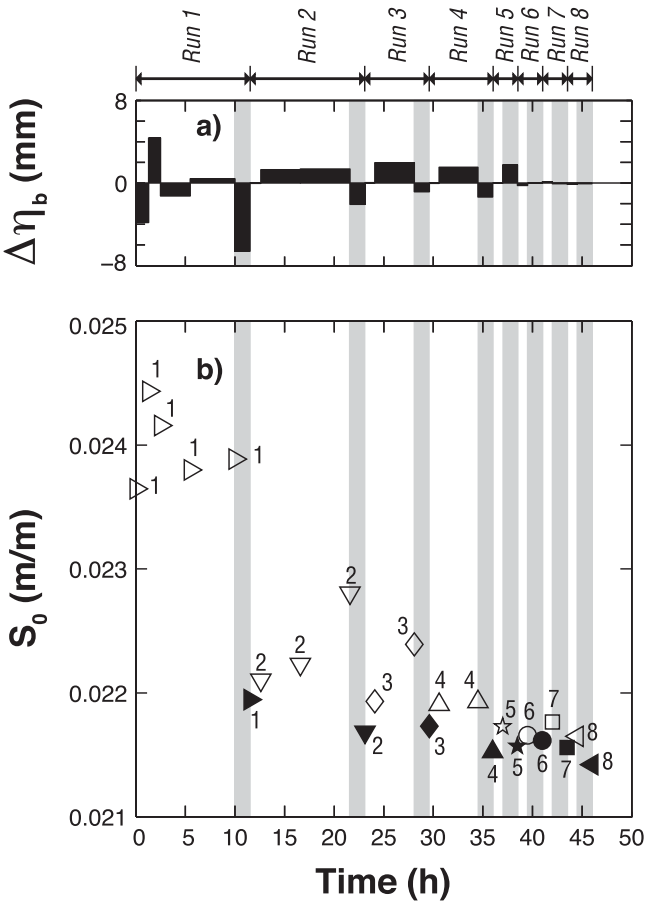

Figure 8. Temporal evolution of (a) the mean bed change (aggradation/degradation) and (b) the bed slope for each run. Different marker types refer to different runs. Open and black markers correspond to data at low flow and water pulses, respectively.

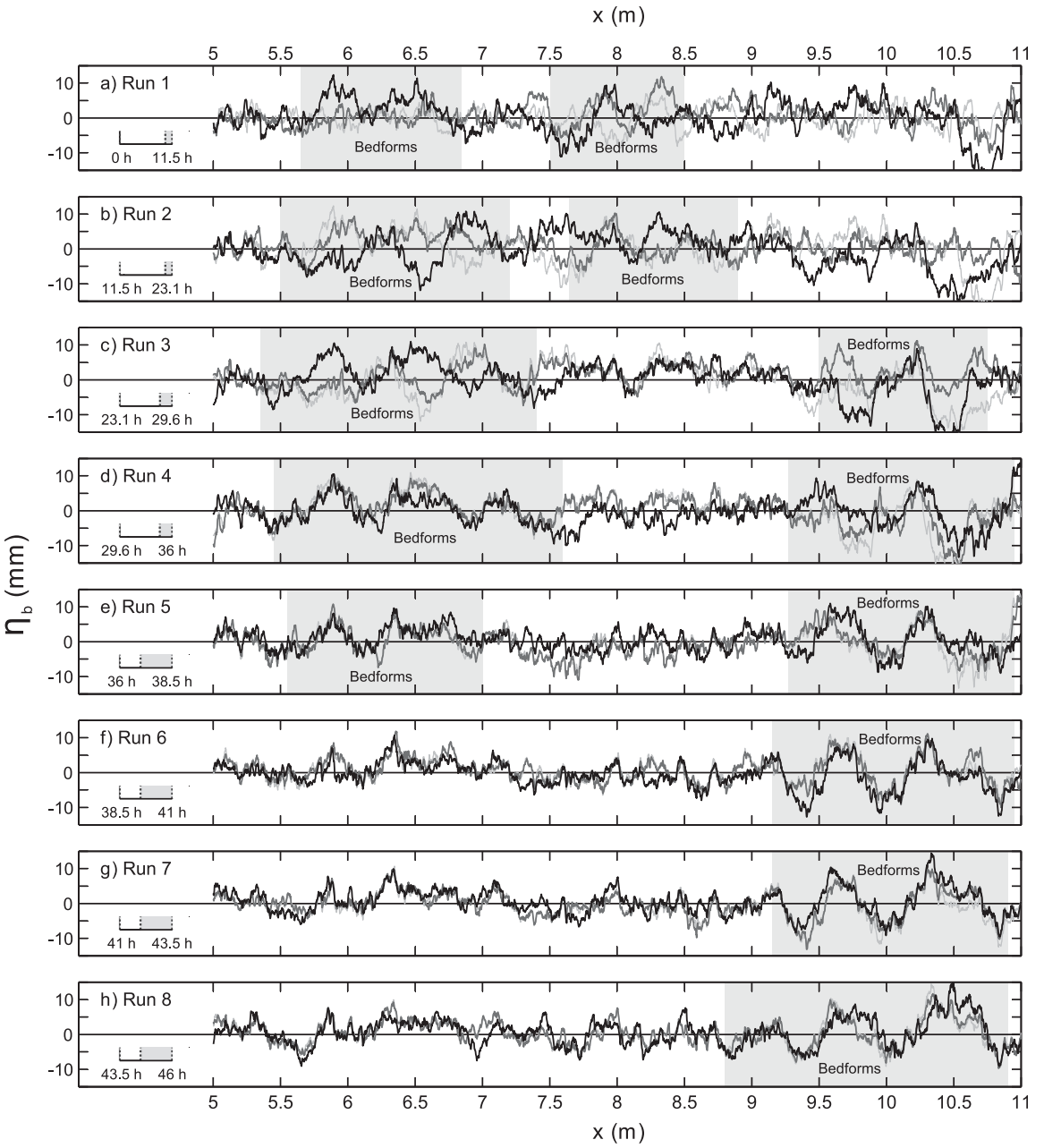

Figure 9. Mean detrended longitudinal profiles for each run. The initial and the final longitudinal profiles at low flow for each run are presented in thin light and dark grey lines, respectively. Thick black curves in each part depict longitudinal profiles at the end of water pulses for each run. These profiles are presented as the starting profiles for the next run (b–h). Grey patches in the bottom left of each part indicate the pulse period and vertical lines represent the selected times for which the longitudinal profiles are selected. Trains of bed forms for each run are identified by grey patches superimposed to the detrended longitudinal profiles. Flow is from right to left.

the average geometric mean diameter of the bed surface throughout the experiment. During this first 10 h of low flow, the mean bed slope S_0 initially increased and then decreased (Figure 8), with a mean value for the period of 0.024 m/m. In all subsequent low-flow periods, the bed aggraded (Figure 8). General bed degradation occurred during high-flow pulses because the same sediment feed rate and texture were supplied for both low and high flows. By the same token, except for the first 10 h at low flow, the channel aggraded during subsequent low-flow runs (Figure 8a). Worth noting is that aggradation was observed for the pulse of run 5 (Figure 8a). However, we think that this aggradation reflects a local aggradation in the bed profile: note that overall trend of the bed profile (characterized by S_0, Figure 8b) was still dominated by degradation, i.e., by a decrease in S_0 during the pulse in run 5. Little degradation was also noticed during pulses for

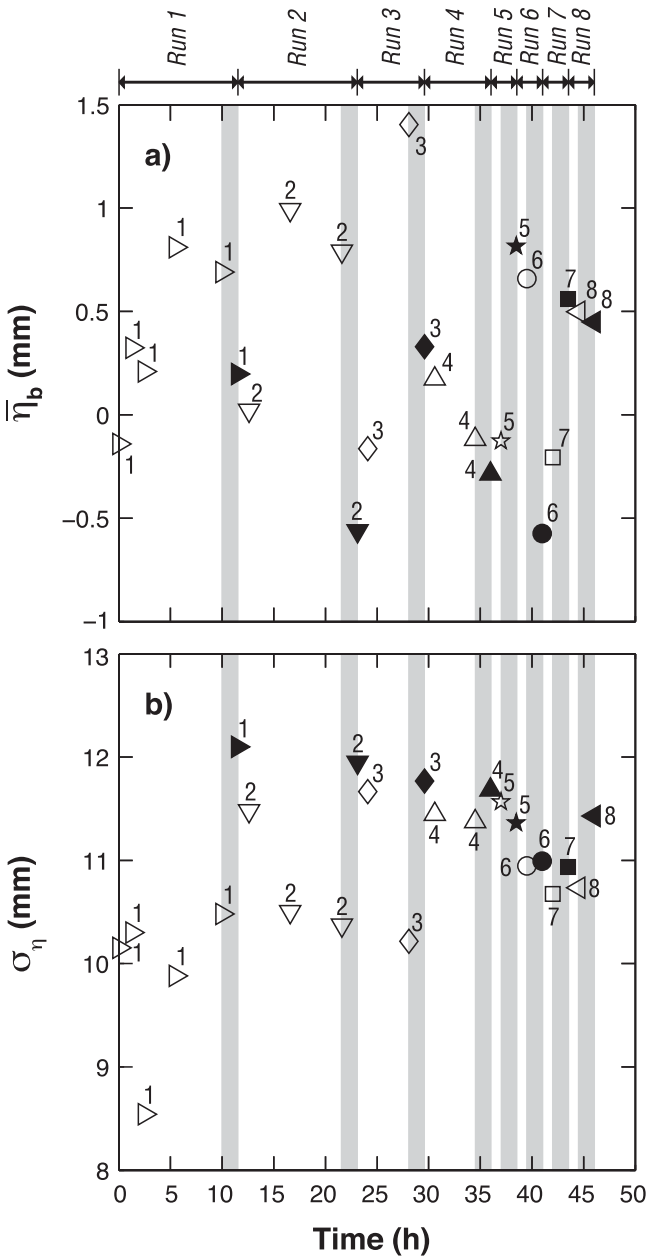

Figure 10. Temporal evolution of (a) the mean bed elevation -η_b and (b) the standard deviation σ_η of the mean detrended bed surfaces. Different marker types refer to different runs. Open and filled markers correspond to data at low flow and water pulses, respectively.

runs 6–8. The overall change in bed elevation during high-flow pulses gradually declined with time (Figure 8a), most of this reduction occurred between pulses of runs 1 and 2. This trend in bed elevation is supported by the decreasing difference in bed slope before and after pulses (Figure 8b). Over time, pulses of high flow had declining effect on channel degradation (Figure 8b): while an 8% decline in the mean channel slope was reported after the first pulse, this drop gradually decreased to 5%, 3%, and 2% after the second, third, and the forth pulses, respectively. Few changes were observed during the last four pulses, when the maximum relative reduction of the mean bed slope was 1%. Bed aggradation rates during low-flow periods (measured in terms of the temporal rate of change of the mean bed slope within the entire low-flow duration) remained approximately constant (Figure 8b). The declining temporal trend of S_0 before and after high-flow pulses therefore reflected the decreasing duration of low-flow periods.

Unlike the minor differences in mean bed elevation during runs (Figure 8a), large local variations of bed elevation are evident between consecutive measurements, especially before and after high-flow pulses (Figure 9). The

maximum differences between consecutive mean detrended longitudinal profiles before and after each high-flow pulse rose from ±15 mm for run 1 to ±18 mm for run 2 (both with a low-flow period $\Delta t_{LF} = 10$ h). These differences in the bed profile declined steadily in later runs: ±17 and ±14 mm for runs 3 and 4, respectively ($\Delta t_{LF} = 5$ h) and from ±12 to ±9 mm from runs 5 to 8 ($\Delta t_{LF} = 1$ h) (Figure 9). Local variations in bed elevation between consecutive mean detrended longitudinal profiles during low-flow periods were of lower magnitude than during high-flow pulses. Local bed variations gradually increased during run 1 (from ±6 to ±11 mm at t = 1.3 h and t = 10 h, respectively). Bed changes ranged from ±9 to ±13 mm during run 2 and dropped for latter runs, from ±9 to ±4 mm. As during high-flow pulses, maximum local differences in detrended bed elevations over the 1 h duration in the last four runs declined from 8 mm (run 5) to 4 mm (run 8).

Detrended longitudinal profiles present patterned irregularities in the bed elevation that were generally identified as bed forms (Figure 9). Bed forms in the first longitudinal profile were clearly observed in two zones: between flume coordinates x = 5.5 and 6.8 m and between x = 7.5 and x = 9.0 m (Figures 3 and 9a). This initial configuration evolves in time according to certain patterns. Sediment deposited on the stoss sides of bed forms increasing the elevation of the troughs during low-flow periods thus smoothing the bed. Simultaneously, the lee sides of bed forms eroded. Both processes resulted in an upstream migration of the bed forms (Figure 9). High-flow pulses disrupted the longitudinal structure of bed forms by enlarging both their wavelengths and amplitudes. For the first three low-flow runs ($\Delta t_{LF} = 10$ h and 5h), $\bar{\eta}_b$, the mean bed elevation of the detrended bed surface, gradually increased (Figure 10a). Because the upstream migration of bed forms took place without significantly altering the bed elevations of their crests (Figure 9), an increase of $\bar{\eta}_b$ is attributed entirely to the deposition of material in troughs between bed forms. The combined effect of (i) relatively constant elevations of the bed form crests (Figure 9) and (ii) the increase of the elevations within troughs (Figures 9 and 10a) throughout low-flow runs resulted in a gradual decline of the bed forms amplitude, reflected by a decrease in the standard deviation of the detrended surfaces σ_η (Figure 10b). High-flow pulses increased the amplitude of the bed forms (Figure 9) which is reflected in the increase in σ_η (Figure 10b). While bed forms were clearly noticed for the last four runs ($\Delta t_{LF} = 1$ h), a more complex and less evident temporal evolution of their magnitude and wavelength were observed (Figure 10b): σ_η slightly decreased during the last four low-flow periods while a small declined was noticed after the pulse in run 5 and nearly no change in σ_η was reported after the high-flow pulse in run 6.

4. Discussion

4.1. Armor Persistence: The Role of Bed Structures

The initial bed upon which these experiments were conducted was conditioned by 280 h of constant flow and varied episodic sediment supply, which resulted in a coarse and structured bed surface (e.g., pebble clusters and cells), development of a sediment wedge, and development of alternate bars downstream of the wedge [*von Flotow*, 2013; *Elgueta*, 2014]. These initial conditions significantly influenced the response of the channel to both low-flow and flood pluses. This initial configuration is comparable to that of natural rivers where flow interacts with the bed and flood history dictates bed configuration [e.g., *Oldmeadow and Church*, 2006; *Ockelford and Haynes*, 2013]. In this sense, our experimental results represent realistic conditions for natural rivers.

Before discussing the persistence or breakup of the initial surface texture throughout the experiment, we aim to characterize its grain-size distribution. The question at hand is whether the surface texture resulting from the previous 280 h-long experiment coarsened to its maximum degree (i.e., static armor). The theoretical grain-size distribution of the static armor, denoted as $f_{a,i}$, associated with the mixture frequency distribution ($f_{bulk,i}$) used in this study (Figure 2) has been estimated following the procedure suggested by *Parker and Sutherland* [1990]:

$$f_{a,i} = \frac{f_{bulk,i} {D_{gi}}^a}{\sum f_{bulk,i} {D_{gi}}^a} \tag{3}$$

where D_{gi} is the geometric mean diameter for each grain size (obtained as $D_{gi} = \sqrt{D_i D_{i+1}}$ where D_i and D_{i+1} are the lower and the upper grain-size bounds or by the arithmetic mean of the bounds of each grain-size class in ψ-scale). a in equation (3) is an exponent initially determined equal to 1.35. A better performance of

equation (3) was obtained by *Parker and Sutherland* [1990] after a was adjusted to 1.12. Using $a = 1.12$ yielded a theoretical particle size distribution of the bed surface statistically similar (K-S at the 0.05 level) to that of the initial conditions of our experiments. Because we observed no statistical difference in bed-surface texture throughout the experiment (Figure 4a), this implies the bed surface had coarsened to its maximum degree for the flows used.

Bed structures were identified on the initial surface following the same procedure outlined by *Church et al*. [1998] and *Hassan and Church* [2000]. These structures were identified by eye as cells, clusters, and transverse and longitudinal structures [*von Flotow*, 2013; *Repetti*, 2014]. The development of a static armor is characterized both by an accumulation of coarse particles on the surface and by the way in which these particles organize themselves into structures that reduce the mobility of surface grains [*Parker*, 2008] and enhance bed stability [*Church et al*., 1998].

The influence of the bed structures and bed forms on bed stability and their response to water pulses are analyzed using measured dimensionless bed load transport rates and associated dimensionless shields shear stresses (Figure 5b). We use the modified sediment transport capacity derived by Meyer-Peter and Müller [*Wong and Parker*, 2006]. This equation, as many other sediment transport capacity formulae, estimates the bulk sediment transport rate for a given mean boundary shear stress. However, MPM equation does not include the presence of mixtures, bed structures, or bed forms. Therefore, a certain degree of uncertainty is associated with its use for a sediment transport rate prediction. However, since the texture of the feed was maintained constant, the flow conditions and the bed-surface texture did not change significantly throughout the experiment (Figures 4a and 5b), it seems reasonable to assume that the degree of uncertainty in the sediment transport predictions is approximately constant throughout the experiments. Therefore, the estimates of the sediment transport rate provided by MPM equation can be used to infer the relative influence of the bed structures during the experiment. Similar approaches have been used by *Dietrich et al*. [1989], *Church et al*. [1998], and *Hassan and Church* [2000]. It was found that sorting processes were affected by the duration of low flow between flood pulses. Since bed load transport is influenced by sediment sorting, the evolution of bed load transport is impacted by the frequency of the water pulses: short interpulse durations reduce the time over which fine material (transported as bed load) can be winnowed. This, in turn, contributes to declining reduction of the bed load transport over time while the sediment storage increases. To this end, we hypothesize that any negative departure in measured q_b^* from the theoretical sediment transport capacity (if the measured value is less than that predicted) is attributed to the presence of bed structures and bed forms, to supply-limited conditions, or to both. Because cumulative volumes of sediment leaving the flume were well below feed volumes (Table 2 and Figure 5), supply limitation is discarded as a potential cause for reduced sediment transport. Therefore, the presence of bed structures and bed forms is the most plausible cause limiting sediment transport rates.

Comparison of τ_b^* calculated for observed dimensionless bed load transport q_b^* (Figures 5b) with the measured values provides an estimate of the percentage of shear stress absorbed by bed structures and bed forms. Our calculations suggest that, on average, bed structures and bed forms reduced about 20% of shear stress during the first low-flow period (14% for the longitudinal profile obtained after 1 h at low flow). Forty percent reduction in shear stress is obtained if the *Wilcock and Crowe* [2003] equation (W-C) is used. During this period, the presence of bed forms was limited to two spots covering less than half of the flume length (Figure 9a). Thus, this reduction was likely caused by the presence of bed structures (with a minor implication of the bed forms in this reduction). Low sediment transport rates registered throughout the first low-flow period strengthen this idea. The proportion of shear stress reduced by bed structures and bed forms rises to about 33% during the first high-flow pulse (20% if the W-C is used). By that time, bed forms were widespread across the channel bed (Figure 9a). Therefore, we cannot discern whether bed forms or bed structures were the principle cause of this high proportion of the shear stress consumed during the first high-flow pulse. The average percentage of shear stress absorbed by structures/bed forms declines to 10% when using the MPM equation—and to 20% if W-C is used—during the second low-flow period. Bed forms were more prevalent in run 2 than in run 1 at low flow (Figures 9a and 9b). Therefore, bed forms, rather than bed structures likely played a larger role in reducing shear stress. These results imply that, regardless of sediment transport equation used—MPM or W-C—the part of the shear stress absorbed by bed structures and bed forms was reduced by half after the first pulse. In fact, these magnitudes can be interpreted

Table 3. Results of the Dimensionless Reference Shear Stress for Each Grain Size for Runs 1 and 2–8 at Low Flow

	τ_{ri}^*	
D_i (mm)	Run 1	Runs 2–8
53.8	0.013	0.012
38.1	0.019	0.016
26.9	0.028	0.023
19	0.040	0.032
13.4	0.055	0.046
9.51	0.077	0.066
6.73	0.11	0.092
4.76	0.15	0.13
3.36	0.22	0.18
2.38	0.29	0.26

as a minimum reduction of the shear stress by bed structures. On one hand, in order to meet the increase the sediment transport at low flow during run 2 compared to that in run 1, the effective shear stress (the total boundary shear stress minus the fraction taken by bed forms and/or bed structures) should be higher in run 2 than in run 1. However, and as stated above, bed forms were more present in run 2 than in run 1 at low flow (Figures 9a and 9b). Therefore, if bed forms are considered, the fraction of the shear stress absorbed by bed structures should be higher than that obtained above. Finally, if bed structures did not play any role in reducing the total boundary shear stress and all the reduction was caused by the presence of bed forms, the combined effect of (i) higher presence of bed forms in run 2 than in run 1 at low flow and (ii) the higher sediment transport rate in run 2 than in run 1 could not be explained based on excess of boundary shear stress with respect the critical condition. For all this, we think that bed forms played a secondary role in reducing shear stress. The magnitude of shear stress reduction we computed is in agreement with the results obtained by *Hassan and Church* [2000], who report that the percentage of shear stress reduced by bed structures ranges from 15% and 50% of the total boundary shear stress.

The first pulse of high flow likely dislodged coarse particles (which in a structured bed only move sporadically) [*Hassan and Church*, 2000], opened structures, and led to reduced bed stability [*Church et al*., 1998]. Such loosening of structures resulted in an increase of bed load transport, which in turn reduces the differences between measurements and predicted bed load transport (Figure 5b). The drop in the percentage of shear stress reduced by the presence of bed structures/bed forms between runs 1 and 2 at low flow (from about 20% to 10% or from 40% to 20% if MPM and W-C are used, respectively) partly accounts for the nearly threefold increase in average sediment transport rate (Table 2). However, even when bed structures were loosened, armor texture was still present (Figure 4a). As pointed out by *Parker et al*. [1982], such preservation is possible because on an armored surface, even though there is continuous exchange of particles between the surface and the bed load, sediment transport takes place over small areas of the bed.

The bed surface structures loosening and its effects on the sediment transport rates before and after the first high-flow pulse have been analyzed by means of the evolution of the dimensionless reference shear stress τ_{ri}^* associated with the ith grain size. This dimensionless shear stress is usually associated with a low but quantifiable sediment transport rate W_i^* [e.g., *Parker and Klingeman*, 1982; *Parker*, 1990; *Wilcock and Crowe*, 2003], where $W_i^* = q_{bi}^* / \left(F_i \tau_i^{*3/2} \right)$ being q_{bi}^*, F_i and τ_i^* the Einstein number—equation (1)—the surface fraction frequency and the Shield dimensionless shear stress—equation (2)—associated with the grain size D_i, respectively. Mean values of the reference shear stress for grain sizes coarser than 2 mm have been obtained by fitting lines to our experimental results of W_i^* versus τ_i^* and imposing $W_i^* = 0.002$. Similar methodology had been previously applied by *Mao* [2012], *Guney et al*. [2013], and *Waters and Curran* [2015] among others. A 15% reduction of the mean dimensionless reference shear stress for during runs 2–8 at low flow compared to that during run 1 for the same flow rate was observed (Table 3). Differences in particle entrainment between rising and falling limbs of stepped hydrographs have been associated with changes in particle rearrangement [*Mao*, 2012] or to complex bed surface with presence of gravel and sand patches [*Waters and Curran*, 2015]. In our experiment, the reduction in the reference shear stress was likely produced by the loosening of bed structures present on the channel [*Elgueta*, 2014; *von Flotow*, 2013]. This reduction in reference shear stress contributed to the threefold increase of bed load transport at low flow after the first water high-flow pulse.

4.2. Surface Sorting and Bed Load Transport Rates: Influence of Sediment Storage

Another question that arises concerns is what are the reasons for the gradual decline in bed load transport rate during high-flow pulses under likely transport-limited conditions (mainly because of the storage of sediment during the previous experiment that ensured high sediment availability) (Figure 5b and Table 2). Dimensionless sediment transport rates appear disconnected from measured Shields numbers (Figure 5a and Table 2). The greatest values of q_b^* registered during the first and second high-flow pulses occurred

with 20% drop in τ_b^* was noticed between them, and a subsequent gradual in transport rate coincided with a relatively constant value of τ_b^* ($\sim$0.062). Thus, another physical explanation must account for the gradual decline in sediment transport rates with time.

One explanation for this decline in bed load transport is found in the way that sediment sorted along the flume. A sharp increase in the sorting slope (measured in terms of the armor ratio of the geometric mean size) was observed after the first high-flow pulse (Figure 4b). Thus, downstream fining increased after this pulse. Because averaged geometric mean size remained stable throughout the run (Figure 4a), an increase in the sorting slope implies that more fine material was deposited in the lower reach of the flume. This material, intrinsically more mobile, along with the loosening of surface structures, contributed to the increase of sediment transport at low flow in run 2 (Table 2). During this low-flow period, bed load transport and its texture were well below and finer than the sediment feed rate (Figures 5a and 6b). This implies that sediment-supplied fractions coarser than the median grain size accumulated on the surface at low flow. The introduced material most likely concentrated in a wedge of material near the upstream end of the flume [*Wilcock*, 2001; *von Flotow*, 2013; *Elgueta*, 2014; *Ferrer-Boix and Hassan*, 2014]. It contributed to the gradual increase in sorting slope (downstream fining) throughout the second period of low flow (Figure 4b), which again implied a higher presence of fine particles in the distal reach of the flume. Thus, a high proportion of fine material was available for transport during the second high-flow pulse (Table 2). In contrast to the first high-flow pulse, the second pulse reduced the sorting slope (Figure 4b), that is, sediment became less fine longitudinally. This change in sorting slope can be interpreted as a partial removal of the upstream wedge of material, because some coarse particles moved downstream. The same sequence of the sediment transport rate, and sediment sorting on the bed surface described for run 2 is repeated for runs 3 and 4, where the duration of the low-flow periods (5 h) allowed some increase in downstream fining (Figure 4b). The duration of subsequent low-flow periods ($\Delta t_{LF} = 1$ h) was not long enough to longitudinally sort sediment. This lack of longitudinal sorting limited the availability of fine sediment in the lower reaches of the flume which can be transported by high-flow pulses. This reduction in fine sediment availability, which arises from the short duration of the low-flow periods,) was the most important cause of the gradual decline of bed load transport (Figure 5a and Table 2). These results imply that in natural mountain streams, sediment storage and bed-surface texture can remain stable under low to moderate flood events. Under these events, the time elapsed between floods might contribute, however, to reduce the sediment storage: the longer the time between floods, the most likely the reduction in sediment storage.

Guney et al. [2013] claimed that good predictions of bed load transport under unsteady flows must take armor ratio into consideration. *Waters and Curran* [2015] highlighted the effects of the antecedent flow conditions and the complexity of the surface configuration in sediment transport patterns. These effects were embedded in the reference shear stress. Our research demonstrates, however, that sediment sorting along the bed is also an important factor for bed load transport predictions and for channel adjustments. Similar conclusions were derived from two studies on river equilibrium and on bank erosion [*Pitlick et al*., 2008, 2013, respectively]. As in our experiments, they concluded that subtle changes in boundary shear stresses or bed grain-size distribution along the channel can have large effects on sediment transport. Further, they found that these changes might not directly correlate in adjustments of bed profile.

Although not studied in these experiments, the magnitude of the floods might contribute to reduce of in-channel sediment storage. Low and high-flow rates in our experiments were similar to bank full and 1.4 times bankfull discharge of a small mountain stream, respectively. We believe that the sediment stored in similar rivers might be disturbed under stronger flood events.

5. Conclusions

We examined changes of gravel bed channels to a series of experimentally manipulated hydrograhs. Hydrographs consisted of low-flow periods of variable duration followed by a high-flow pulse (flood) of 1.5 h duration. Our experiments were preceded by a 280 h-long experiment that produced an armored and structured surface texture and significant sediment storage along the channel. This configuration, which can be found in mountain gravel bed rivers, constituted the initial condition for our runs.

Persistently waning cycles of bed aggradation and degradation were observed during recurrent low-flow and high-flow pulses. An invariant armored surface texture persisted throughout the experiment. However,

particles that formed textural structures at the beginning of the experiments were partially dislodged, reducing particle imbrication, and permitting an increase in bed load transport. Disruptions of textural structures was particularly notable after the first high-flow pulse when the proportion of boundary shear stress reduced by the bed structures dropped from 20% during the first low-flow period to 10% during the second low-flow period. Further, a 15% reduction of the reference dimensionless shear stress after the first high-flow pulse contributed to increase sediment transport rate during run 2 at low flow.

Throughout the experiment, the bed-surface texture fined in the downstream direction. We found that the degree of downstream fining was affected by the duration of low-flow periods between high-flow pulses: the longer the low-flow period, the greater the downstream fining. By contrast, the degree of downstream fining was less following high flow and the degree to which it lessened was related to the duration of the preceding low flow. Changes in sorting processes related to the duration of low flow caused a gradual decline of the rate of bed load transport during high-flow pulses, which was the most important channel adjustment registered throughout the experiment.

Acknowledgments
We thank Jon Major, John Pitlick, and two other anonymous reviewers for their constructive comments and suggestions that helped us improve the manuscript. The readers can freely access the data from this paper by contacting the first author.

References

Alexandrov, Y., J. B. Laronne, and I. Reid (2007), Intra-event and inter-seasonal behaviour of suspended sediment in flash floods of the semi-arid northern Negev, Israel, *Geomorphology*, *85*, 85–97, doi:10.1016/j.geomorph.2006.03.013.

Andrews, E. D., and D. C. Erman (1986), Persistence in the size distribution of surficial bed material during an extreme snowmelt flood, *Water Resour. Res.*, *22*(2), 191–197, doi:10.1029/WR022i002p00191.

Church, M., and M. A. Hassan (2002), Mobility of bed material in Harris Creek, *Water Resour. Res.*, *38*(11), 1237, doi:10.1029/2001WR000753.

Church, M., M. A. Hassan, and J. F. Wolcott (1998), Stabilizing self-organized structures in gravel-bed stream channels: Field and experimental observations, *Water Resour. Res.*, *34*(11), 3169–3179, doi:10.1029/98WR00484.

Clayton, J. A., and J. Pitlick (2008), Persistence of the surface texture of a gravel-bed river during a large flood, *Earth Surf. Processes Landforms*, *33*, 661–673, doi:10.1002/esp.1567.

Dietrich, W. E., J. W. Kirchner, H. Ikeda, and F. Iseya (1989), Sediment supply and the development of the coarse surface layer in gravel-bedded rivers, *Nature*, *340*, 215–217, doi:10.1038/340215a0.

Elgueta, M. A. (2014), Channel adjustment of a gravel-bed stream under episodic sediment supply regimes, MS thesis, 76 pp., Univ. of B. C., Vancouver, Canada.

Ferrer-Boix, C., and M. A. Hassan (2014), Influence of the sediment supply texture on morphological adjustments in gravel-bed rivers, *Water Resour. Res.*, *50*, 8868–8890, doi:10.1002/2013WR015117.

Ferrer-Boix, C., J. P. Martín-Vide, and G. Parker (2014), Sorting of a sand–gravel mixture in a Gilbert-type delta, *Sedimentology*, *62*, 1446–1465, doi:10.1111/sed.12189.

Guney, M., G. Bombar, and A. Aksoy (2013), Experimental study of the coarse surface development effect on the bimodal bed-load transport under unsteady low conditions, *J. Hydraul. Eng.*, *139*(1), 12–21, doi:10.1061/(ASCE)HY.1943-7900.0000640.

Hassan, M. A., and M. Church (2000), Experiments on surface structure and partial sediment transport on a gravel bed, *Water Resour. Res.*, *36*(7), 1885–1895, doi:10.1029/2000WR900055.

Hassan, M. A., M. Church, T. E. Lisle, F. Brardinoni, L. Benda, and G. E. Grant (2005), Sediment transport and channel morphology of small, forested streams, *J. Am. Water Resour. Assoc.*, *41*, 853–876.

Hassan, M. A., R. Egozi, and G. Parker (2006), Experiments on the effect of hydrograph characteristics on vertical grain sorting in gravel bed rivers, *Water Resour. Res.*, *42*, W09408, doi:10.1029/2005WR004707.

Hassan, M. A., B. J. Smith, D. L. Hogan, D. S. Luzi, A. E. Zimmermann, and B. C. Eaton (2008), Sediment storage and transport in coarse bed streams: Scale considerations, in *Gravel-Bed Rivers VI: From Process Understanding to River Restoration*, edited by M. Rinaldi, H. Habersack, and H. Piégay, Elsevier, Amsterdam, Netherlands.

Haynes, H., and G. Pender (2007), Stress history effects on graded bed stability, *J. Hydraul. Eng.*, *133*(4), 343–349, doi:10.1061/(ASCE)0733-9429(2007)133:4(343).

Humphries, R., J. G. Venditti, L. S. Sklar, and J. K. Wooster (2012), Experimental evidence for the effect of hydrographs on sediment pulse dynamics in gravel-bedded rivers, *Water Resour. Res.*, *48*, W01533, doi:10.1029/2011WR010419.

Kleinhans, M. G. (2005), Grain-size sorting in grainflows at the lee side of deltas, *Sedimentology*, *52*, 291–311, doi:10.1111/j.1365-3091.2005.00698.x.

Kuhnle, R. (1989), Bed-surface size changes in gravel-bed channel, *J. Hydraul. Eng.*, *115*(6), 731–743, doi:10.1061/(ASCE)0733-9429(1989)115:6(731).

Lee, K. T., Y.-L. Liu, and K.-H. Cheng (2004), Experimental investigation of bedload transport processes under unsteady low conditions, *Hydrol. Processes*, *18*(13), 2439–2454, doi:10.1002/hyp.1473.

Lisle, T. E., F. Iseya, and H. Ikeda (1993), Response of a channel with alternate bars to a decrease in supply of mixed-size bed load: A flume experiment, *Water Resour. Res.*, *29*(11), 3623–3629, doi:10.1029/93WR01673.

Madej, M. A. (2001), Development of channel organization and roughness following sediment pulses in single-thread, gravel bed rivers, *Water Resour. Res.*, *37*(8), 2259–2272, doi:10.1029/2001WR000229.

Madej, M. A., D. G. Sutherland, T. E. Lisle, and B. Pryor (2009), Channel responses to varying sediment input: A flume experiment modeled after Redwood Creek, California, *Geomorphology*, *103*, 507–519, doi:10.1016/j.geomorph.2008.07.017.

Mao, L. (2012), The effect of hydrographs on bed load transport and bed sediment spatial arrangement, *J. Geophys. Res.*, *117*, F03024, doi:10.1029/2012JF002428.

Martin, R. L., and D. J. Jerolmack (2013), Origin of hysteresis in bed form response to unsteady flows, *Water Resour. Res.*, *49*, 1314–1333, doi:10.1002/wrcr.20093.

Ockelford, A.-M., and H. Haynes (2013), The impact of stress history on bed structure, *Earth Surf. Processes Landforms*, *38*(7), 717–727, doi:10.1002/esp.3348.

Oldmeadow, D. F., and M. Church (2006), A field experiment on streambed stabilization by gravel structures, *Geomorphology*, *78*(3–4), 335–350, doi:10.1016/j.geomorph.2006.02.002.

Parker, G. (1990), Surface-based bedload transport relation for gravel rivers, *J. Hydraul. Res.*, *28*(4), 417–436.
Parker, G. (2008), Transport of gravel and sediment mixtures, in *Sedimentation Engineering. Processes, Measurements, Modeling and Practice*, edited by M. H. García, pp. 165–251, Am. Soc. of Civ. Eng., Reston, Va.
Parker, G., and P. Klingeman (1982), On why gravel bed streams are paved, *Water Resour. Res.*, *18*(5), 1409–1423, doi:10.1029/WR018i005p01409.
Parker, G., and A. J. Sutherland (1990), Fluvial armor, *J. Hydraul. Res.*, *28*(5), 529–544.
Parker, G., S. Dhamotharan, and H. Stefan (1982), Model experiments on mobile, paved gravel bed streams, *Water Resour. Res.*, *18*(5), 1395–1408, doi:10.1029/WR018i005p01395.
Parker, G., M. A. Hassan, and P. Wilcock (2008), Adjustment of the bed surface size distribution of gravel-bed rivers in response to cycled hydrographs, in *Gravel-Bed Rivers VI: From Process Understanding to River Restoration*, edited by H. Habersack, H. Piégay, and M. Rinaldi, pp. 241–289, Elsevier, Amsterdam, Netherlands.
Pitlick, J. (1994), Relation between peak flows, precipitation, and physiography for five mountainous regions in the western, *J. Hydrol.*, *158*, 219–240, doi:10.1016/0022-1694(94)90055-8.
Pitlick, J., E. R. Mueller, C. Segura, R. Cress, and M. Torizzo (2008), Relation between flow, surface-layer armoring and sediment transport in gravel-bed rivers, *Earth Surf. Processes Landforms*, *33*(8), 1192–1209, doi:10.1002/esp.1607.
Pitlick, J., J. Marr, and J. Pizzuto (2013), Width adjustment in experimental gravel-bed channels in response to overbank flows, *J. Geophys. Res.*, *118*, 553–570, doi:10.1002/jgrf.20059.
Pryor, B. S., T. E. Lisle, M. D. Sutherland, and D. Hilton (2011), Transport and storage of bed material in a gravel-bed channel during episode of aggradation and degradation: A field and flume study, *Earth Surf. Processes Landforms*, *36*, 2028–2041, doi:10.1002/esp.2224.
Reid, I., L. E. Frostick, and J. T. Layman (1985), The incidence and nature of bedload transport during flood flows in coarse-grained alluvial channels, *Earth Surf. Processes Landforms*, *10*(1), 33–44, doi:10.1002/esp.3290100107.
Repetti, M. (2014), Bed surface adjustments to episodic sediment supply in mountain streams, MS thesis, 84 pp., Univ. degli Studi di Trento, Italy.
Ryan, S. E., L. S. Porth, and C. A. Troendle (2005), Coarse sediment transport in mountain streams in Colorado and Wyoming, USA, *Earth Surf. Processes Landforms*, *30*(3), 269–288, doi:10.1002/esp.1128.
Seal, R., C. Paola, G. Parker, J. Southard, and P. R. Wilcock (1997), Experiments on downstream fining of gravel: I. Narrow-channel runs, *J. Hydraul. Eng.*, *123*(10), 874–884, doi:10.1061/(ASCE)0733-9429(1997)123:10(874).
Vanoni, V. A. (1975), *Sedimentation Engineering, ASCE Manuals and Reports on Engineering Practice 54*, Am. Soc. of Civ. Eng., N. Y.
Vericat, D., R. J. Batalla, and C. Garcia (2006), Breakup and reestablishment of the armour layer in a large gravel-bed river below dams: The lower Ebro, *Geomorphology*, *76*(1–2), 122–136, doi:10.1016/j.geomorph.2005.10.005.
von Flotow, C. (2013), Temporal adjustments of a streambed following an episodic sediment supply regime, MS thesis, 146 pp., Univ. of B. C., Vancouver, Canada.
Wang, T., and X. Liu (2009), The breakup of armor layer in a gravel-bed stream with no sediment supply, in *Advances in Water Resources and Hydraulic Engineering: Proceedings of 16th IAHR-APD Congress and 3rd Symposium of IAHR-ISHS*, edited by C. Zhang and H. Tang, pp. 79–90, Springer, Berlin.
Waters, K. A., and J. C. Curran (2015), Linking bed morphology changes of two sediment mixtures to sediment transport predictions in unsteady flows, *Water Resour. Res.*, *51*, 2724–2741, doi:10.1002/2014WR016083.
Wilcock, P. R. (2001), The flow, the bed, and the transport: Interaction in flume and field, in *Gravel-Bed Rivers V*, edited by M. P. Mosley, pp. 183–220, N. Z. Hydrol. Soc., Wellington.
Wilcock, P. R., and J. C. Crowe (2003), Surface-based transport model for mixed-size sediment, *J. Hydraul. Eng.*, *129*(2), 120–128, doi: 10.1061/(ASCE)0733-9429(2003)129:2(120).
Wilcock, P. R., and T. De Temple (2005), Persistence of armor layers in gravel-bed streams, *Geophys. Res. Lett.*, *32*, L08402, doi:10.1029/2004GL021772.
Wilcock, P. R., and B. W. McArdell (1993), Surface-based fractional transport rates: Mobilization thresholds and partial transport of a sand gravel sediment, *Water Resour. Res.*, *29*(4), 1297–1312, doi:10.1029/92WR02748.
Wong, M., and G. Parker (2006), Reanalysis and correction of bed-load relation of Meyer-Peter and Müller using their own database, *J. Hydraul. Eng.*, *132*, 1159–1168, doi:10.1061/(ASCE)0733-9429(2006)132:11(1159).
Zimmermann, A., M. Church, and M. A. Hassan (2010), Step-pool stability: Testing the jammed state hypothesis, *J. Geophys. Res.*, *115*, F02008, doi:10.1029/2009JF001365.